Ab initio study of the magnetic ordering in Si/Mn digital alloys

M. M. Otrokov,[1,2] A. Ernst,[1,*] V. V. Tugushev,[3,4,5] S. Ostanin,[1] P. Buczek,[1] L. M. Sandratskii,[1] G. Fischer,[6] W. Hergert,[6] I. Mertig,[1,6] V. M. Kuznetsov,[2] and E. V. Chulkov[4,5]

[1]*Max-Planck-Institut für Mikrostrukturphysik, Weinberg 2, D-06120 Halle, Germany*

[2]*Physics Department, Tomsk State University, Pr. Lenina 36, 634050 Tomsk, Russia*

[3]*RRC Kurchatov Institute, Kurchatov Square 1, 123182 Moscow, Russia*

[4]*Donostia International Physics Center (DIPC), P. de Manuel Lardizabal 4, San Sebastián, 20018 Basque Country, Spain*

[5]*Departamento de Física de Materiales, Facultad de Ciencias Químicas, UPV/EHU and Centro de Física de Materiales (CFM) (CSIC-UPV/EHU), Apdo. 1072, San Sebastián, 20080 Basque Country, Spain*

[6]*Institut für Physik, Martin-Luther-Universität Halle-Wittenberg, D-06099 Halle, Germany*

(Received 26 July 2011; revised manuscript received 22 September 2011; published 31 October 2011)

We present a first-principles study of the electronic structure and exchange interactions in Si/Mn digital magnetic alloy (DMA) consisting of Mn monolayers embedded in a Si matrix stacking along [001] direction. The main focus of our study is on the dependence of magnetic properties on the morphology of the Mn monolayer. Three different structural models for the Mn monolayer are considered: manganese in substitutional (i), interstitial (ii), and both interstitial and substitutional (iii) positions. The atomic positions in Si/Mn DMA are determined by means of the VASP code and then serve as input for multiple-scattering calculations of the electronic and magnetic structure. The magnetic force theorem is used to evaluate the exchange coupling parameters. A Heisenberg model based on those parameters is used to estimate magnon frequencies and magnetic phase-transition temperatures for different anisotropies. The magnetic properties of Si/Mn DMA are found to be strongly dependent on the underlying crystalline structure.

DOI: 10.1103/PhysRevB.84.144431 PACS number(s): 75.70.Rf, 73.20.At, 68.37.Ef, 68.43.−h

I. INTRODUCTION

The magnetism of silicon-based dilute alloys with transition metals (TMs) is a long-standing problem. It is well known that the relatively low solubility of TMs in silicon prevents the development of stable magnetic order above room temperature.[1,2] Usually, TMs strongly react with silicon, forming different silicides, which are nonmagnetic or weakly magnetic materials.[3,4] However, there exist some remarkable exceptions,[5] such as Si:Mn dilute alloys, where a variety of magnetic properties was observed.[6] There are only a few works investigating the magnetic order in Si:Mn dilute alloys, despite the fact that these systems belong to the highly studied class of dilute magnetic semiconductors (DMSs) and present a great interest due to their potential compatibility with materials of the mainstream silicon technology.

An isolated Mn ion in Si possesses a magnetic moment of about 3 μ_B and mainly occupies a tetrahedral interstitial position in the Si lattice acting as a donor, while a strong hybridization of Mn 3*d* states with 3(s, p) states in Si occurs if the Mn ion occupies a substitutional position acting as an acceptor.[7–9] The situation in the Si:Mn dilute alloys is, however, more complex. These materials attracted more interest after the observation of a ferromagnetic (FM) state with high Curie temperature of about 400 K.[10] This result was obtained in Si:Mn films with a rather low (0.1–0.8 at. %) content of Mn ions. Detailed x-ray and magnetic studies of Si:Mn dilute alloys with low and moderate (from 0.5 to 17.5 at. %) Mn content indicated that, possibly due to an uncontrolled doping process, these systems seem to be very inhomogeneous, and the Mn ions enter not only substitutional or interstitial positions of the Si lattice but also form molecular clusters and precipitates. Furthermore, the results obtained for samples prepared by similar techniques can contradict each other.[10–13] Until now, the mechanism of FM ordering in Si:Mn dilute alloys is far from being understood (see detailed discussion in Ref. 14). Since a FM state was also observed in Si after the implantation of nonmagnetic ions (Ar, Si) or irradiation by neutrons, some authors argued that the ferromagnetism in these alloys is due to paramagnetic defects.[15,16]

Recently, an efficient way to control the doping process has been developed by means of the so-called δ-doping technique,[17] where the dopant is confined on the length scale of the lattice constant and embedded into the matrix of a host material. Such a digital magnetic heterostructure,[18] also called digital magnetic alloy (DMA), contains discrete magnetic layers (monolayers or submonolayers), which are regularly embedded into a nonmagnetic semiconductor host. The distance between magnetic layers usually ranges between 10 and 15 semiconductor layers. The techniques that are applicable to epitaxially deposited semiconductors yield a reasonably narrow doping distribution along the epitaxial growth direction. However, a well-controlled fabrication of Si/Mn DMA is still a challenge. The main problem here is similar to that arising in the case of deposition of Mn layers onto the Si surface, when the formation of a silicide ultrathin interface at the boundary between the Si substrate and the Mn layer destroys the magnetic overlayer homogeneity.[19–22] Nevertheless, under suitable growth conditions, Mn can form a two-dimensional row-like structure, which could be useful for achieving δ-layer doping of silicon by manganese.[20] In this study, Mn was found to be incorporated into Si as an interstitial dopant in good agreement with recent first-principles calculations.[23–25] The interstitial Mn was also observed in thin films irradiated by ultraviolet light releasing metal species into the semiconductor substrate.[26] Meanwhile, molecular beam epitaxy produces samples with mostly substitutional Mn in

the Si matrix.[27] Thus, the Mn dopants in Si were found in both substitutional and interstitial positions, depending critically on the growth technique used.

Electronic and magnetic properties of DMAs differ substantially from that of DMSs with random distribution of the impurity atoms. The electronic structure of DMAs is very complex and is characterized by the presence of both strongly correlated narrow bands and weakly correlated wide bands. The presence of the magnetic metal layers leads to the formation of spin-polarized quasi-two-dimensional bands, which strongly affect the magnetic properties of these materials.[28–31]

According to the experimental data, available mostly for the $A^{III}B^{V}$/Mn DMAs, magnetic δ-layers are essentially smeared in the perpendicular direction[32–34] and can contain clusters and secondary phases.[35] Besides, Mn atoms are always present at the background level in the undoped semiconductor spacers.[36,37] The mentioned morphological peculiarities of real DMAs evidently cannot be captured all at once within the frame of the density functional theory (DFT). Under certain simplifications, the first-principles simulations nevertheless can provide useful information about crystalline, electronic, and magnetic properties of these complex systems. Indeed, several recent DFT-based approaches for systems with imperfections or disorder, ranging from the estimation of the defect formation energies (see, e.g., Ref. 38) to the nonlocal coherent-potential approximation,[39] can give a deeper level of insight into these systems. However, even within the ideal DMA model, containing atomically flat TM monolayers (MLs), it is possible to understand and explain certain important experimental features. For example, in the limit of very thick spacers, the critical temperature obtained for the ideal DMA can be qualitatively associated with the temperature of the magnetic ordering onset in the TM-enriched core region of smeared δ-layer. Nevertheless, some important issues are still to be resolved at the level of this simple model.[29]

First-principles studies shed significant light on the magnetic structure of DMAs. Recently, it was demonstrated that the Mn ML embedded in Si or Ge should form a two-dimensional half-metal with 100% spin polarization at the Fermi energy.[28,40–46] Two models were proposed, in which Mn occupies either substitutional (Mn_S)[40] or interstitial positions (Mn_I).[41] The former model favors the half-metallic and FM solution, whereas the latter energetically favors half-metallicity only for the Mn_I occupancy of 0.25 ML in Si. On the other hand, the ground state of Mn_I ML remains FM and highly spin-polarized for the occupancies of 0.5 ML and 1 ML in Si. Thus, these studies show that the Si/Mn and Ge/Mn DMAs are promising materials for further developments.

In this work, we report the results of *ab initio* study of Si/Mn heterostructures focusing in particular on the exchange interactions and magnetic critical temperature, T_C, estimated for the 1 Mn ML embedded in a Si matrix stacking along [001]. Recently, we published a similar study on Ge/Mn digital alloys.[45] The electronic and magnetic properties of Si/Mn DMAs are expected to be different from the properties of Ge/Mn. First, Si has a larger band gap than Ge, which is crucial for the properties of spin waves in the half-metallic systems.[47] Second, atomic relaxations in Si/Mn are stronger than in the Ge/Mn systems, and, therefore, they should influence stronger the electronic and magnetic properties. For thin films MnSi/Si(001), a similar DFT study has been reported recently.[48] However, structurally, electronically, and magnetically the δ-doped Si/Mn heterostructures differ considerably from MnSi/Si(001) thin films.

In this paper, we consider the three distinct growing scenarios: (i) Mn atoms substitute Si atoms, (ii) Mn atoms are incorporated into the interstitial positions, and (iii) Mn atoms form a dense δ-ML occupying simultaneously substitutional and interstitial positions. The first scenario (i) corresponds to the growth model suggested in Refs. 27 and 40, while the second scenario (ii) mimics the studies of Refs. 20,23–25 and 41. The case (iii) of the most dense Mn ML is also possible, since manganese atoms within the δ-layer can bond together via the metallic bonding, which is much stronger than the covalent bonding and can lead to a more close packed structure. All these scenarios are consistent with the recently reported experimental findings for various magnetic semiconductors.[7]

The paper is organized as follows. The computational details are presented in Sec. II. Section III focuses on the structural properties of Si/Mn heterostructures. In Sec. IV we discuss electronic structure and exchange interactions and then present magnon spectra and estimate critical temperature in Sec. V. The concluding remarks close the paper in Sec. VI.

II. COMPUTATIONAL DETAILS

To model the Si_N/Mn DMAs, we used a $(N+1)$-layer-thick tetragonal supercells, composed of N monolayers of Si and one Mn ML. For the latter, the three different Mn configurations were considered. In Fig. 1, each panel shows the possible Mn positions, namely, the substitutional site Mn_S (a), interstitial site Mn_I (b), and the configuration, labeled as IS (c), where Mn atoms occupy both I and S sites. The Si thickness was varied as $N = 7,11,15\ldots$ between 7 and 31 ML. The unit cell vectors **a**, **b**, and **c** are directed along [110], [$\bar{1}$10], and [001], respectively, with $a = b = a_{Si}/\sqrt{2}$ and $c = a_{Si}(N+1)/4$, where $a_{Si} = 5.46$ Å is the equilibrium lattice parameter of the diamond structure Si.

For the structural relaxation we used the Vienna *ab initio* Simulation Package (VASP)[49–51] within the generalized

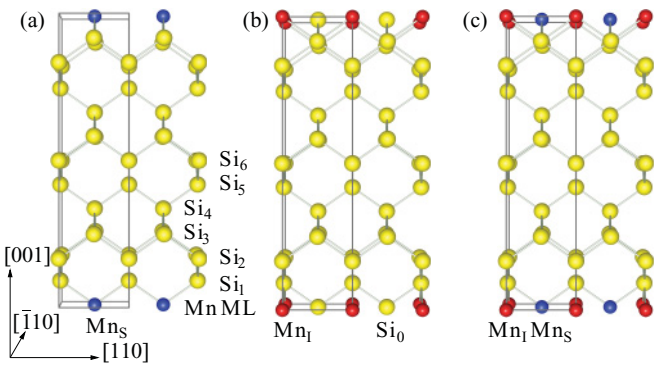

FIG. 1. (Color online) Side view of the 12-ML-thick Si_{11}/Mn superlattices, with the substitutional Mn_S (a) and interstitial Mn_I positions (b). In panel (c), the unit cell with both Mn_S and Mn_I is shown. Yellow spheres represent silicon and blue and red spheres represent Mn_S and Mn_I, respectively. The Si layers are labeled as shown in panel (a).

gradient approximation to exchange-correlation potential.[52] The electron-ion interactions were described by projector-augmented wave pseudopotentials,[53] and the electronic wave functions were represented by plane waves with a cutoff energy of 500 eV. For ionic relaxation, the Γ-centered $4 \times 4 \times 2$ k-point Monkhorst-Pack[54] mesh was used. The use of more dense $6 \times 6 \times 3$ k mesh yield essentially the same atomic positions, within the error <0.5%. To keep the unit cell periodicity we fixed, during the relaxation process, the middle Si ML, namely, monolayer $(N+1)/2$ of each model shown in Fig. 1. In order to inspect the influence of this constraint in small supercells ($N = 3,7$), we allowed every layer to relax and this gives no significant changes in ionic coordinates. The ionic relaxation was performed until the forces were less than 10^{-2} eV/Å.

To explore the interplay between the structural and magnetic properties, we use a multi-code approach. For each completely relaxed atomic configuration obtained by VASP, we performed spin-polarized calculations, within the ferromagnetic and paramagnetic models using our implementation of self-consistent Korringa-Kohn-Rostoker (KKR) method[55] as described elsewhere.[45] The paramagnetic state was simulated using the disordered local moment (DLM) model and the coherent-potential approximation, which are formulated within the multiple-scattering theory.[56,57]

To describe the magnetic properties of Si/Mn heterostructures, we calculated exchange interactions between magnetic moments using the magnetic force theorem as it is implemented within the KKR Green function method:[58]

$$J_{ij} = \frac{1}{4\pi} \int^{\varepsilon_F} d\varepsilon \, \mathrm{Im}\, \mathrm{Tr}_L [\Delta_i(\varepsilon) G^{ij}_{\uparrow}(\varepsilon) \Delta_j(\varepsilon) G^{ji}_{\downarrow}(\varepsilon)]. \quad (1)$$

Here, Tr_L denotes the trace over the angular momentum, $G^{ij}_{\sigma}(\varepsilon)$ is the back scattering operator of a spin σ between sites i and j, and $\Delta_i(\varepsilon) = t^i_{\uparrow}(\varepsilon) - t^i_{\downarrow}(\varepsilon)$ is defined via the single site scattering t matrices t^i_{σ} and is closely related to the exchange splitting corresponding to the magnetic atom i. Exchange parameters calculated for a certain reference state provide usually a reliable hint about the ground state magnetic structure. In our study, exchange parameters were calculated for the FM and DLM reference states. In an ideal Heisenberg system, all calculations should lead to the same results. The difference of the exchange parameters calculated with respect to different reference states can be treated in terms of temperature dependence of the effective interatomic exchange interactions. It is logical to expect that the parameters obtained for the DLM reference state are the better basis for the estimation of the critical temperature of the FM ordering.[59] The use of the $45 \times 45 \times 11$ k-point mesh for the Brillouin zone (BZ) integration enables the convergence of the exchange parameters J_{ij}. More details of the calculational procedure can be found in our recent publication devoted to Ge/Mn digital alloys.[45]

III. STRUCTURAL PROPERTIES

The results of structural relaxations are presented in Fig. 2. The three models considered are labeled as S, I, and IS. Since the intralayer ionic displacements in each ML along [001] were found to be marginal we show only the average displacement

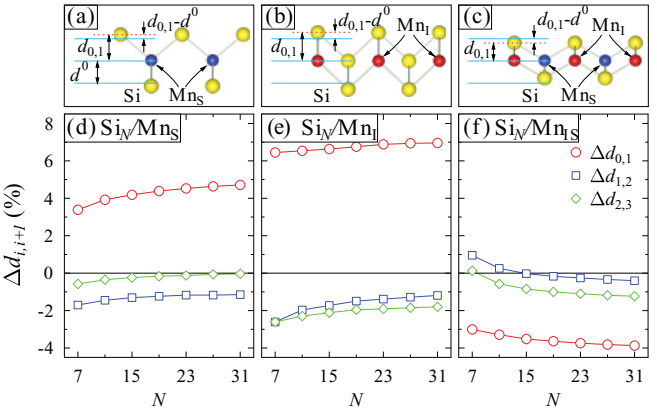

FIG. 2. (Color online) The (110) views of the Si displacements relaxed near the Mn ML in Si_N/Mn, which were calculated for the models S, I, and IS as schematically shown in the panels (a), (b), and (c), respectively. Blue lines correspond to the positions of the (001) atomic planes of ideal Si, whereas all red lines mark the relaxed Si planes adjacent to the Mn plane $i = 0$. In the low panels (d–f), the corresponding relative changes (in %) in the interlayer distances, $\Delta d_{i,i+1} = (d_{i,i+1} - d^0)/d^0$ $(i = 0,1,2)$, are plotted for each model versus the Si thickness N. Here d^0 is the Si-Si interlayer distance along [001] before relaxation, $d_{0,1}$ is the distance between the Mn ML and adjacent Si layers, while $d_{1,2}$ and $d_{2,3}$ are the Si-Si interlayer distances along [001] after relaxation.

calculated for each atomic plane. The unrelaxed interlayer distance along [001] between the Mn ML and adjacent Si is $d_{0,1} = 1.366$ Å. After relaxations, the distance $d_{0,1}$ in Si_N/Mn_S and Si_N/Mn_I increases to the values of 1.420–1.456 Å [see Figs. 2(a) and 2(b)]. Besides, $d_{0,1}$ gradually increases with increasing the number N of Si monolayers. In particular, for Mn_S $\Delta d_{0,1}$ increases from 3.2% to 4.7% when N changes from 7 to 31 ML [see Fig. 2(d)]. This effect can be attributed to the formation of equilibrium Si–Mn_S bond length within the superlattice geometry. The Si-Si interlayer distances $\Delta d_{1,2}$ and $\Delta d_{2,3}$ are only slightly reduced after structural relaxations.

In Si_N/Mn_I the separation $d_{0,1}$ increases significantly with increasing N and $\Delta d_{0,1}$ approaches the value of 7 % at $N = 31$ as shown in Fig. 2(e). In this case, the relaxation mechanism becomes rather complicated since apart from the Si-Mn_I bond length formation there is the volume effect which leads to extra repulsion of Si planes due to the presence of Mn interstitials. For the same reason, Si-Si interlayer distances show slightly larger relaxations than in case of Si_N/Mn_S. The relaxation mechanism of the models S and I cannot be applied to the case of Mn_{IS}, which is shown in Figs. 2(c) and 2(f). For the two former models, the shortest Mn-Mn distance is 3.865 Å, while in the case of Mn_{IS} the in-plane Mn-Mn distance of 2.733 Å is significantly shorter. As a result, the Mn ML in Si_N/Mn_{IS} becomes strongly metallic while the Si relaxation is completely different compared to models S and I. This effect of relaxations is similar to that in Si/Fe DMA, where the Fe layers also exhibit strong metallic character.[60]

In the next section we shall discuss magnetic properties of Si_N/Mn heterostructures. Generally, magnetic properties of silicon materials doped with TMs are strongly affected by the crystallographic environment of the impurity. In the case of δ-doped Si/Mn heterostructures, this will be fully governed

TABLE I. The radii of the coordination spheres for the Mn atom in unrelaxed Si_{11}/Mn_S, Si_{11}/Mn_I, and Si_{11}/Mn_{IS} as well as local magnetic moments for FM and DLM solutions (N2, nearest neighbors; N3, next nearest neighbors,...).

				Si_{11}/Mn_{IS}	
		Si_{11}/Mn_S	Si_{11}/Mn_I	Mn_S	Mn_I
m (μ_B)	FM	3.152	2.722	2.590	1.554
	DLM	3.046	2.286	2.586	2.512
R (Å)	N2	2.367 (4 Si_1)	2.367 (4 Si_1)	2.367 (4 Si_1)	2.367 (4 Si_1)
	N3	3.865 (4 Mn_S + 8 Si_2)	2.733 (4 Si_0 + 2 Si_2)	2.733 (4 Mn_I)	2.733 (4 Mn_S + 2 Si_2)
	N4	5.466 (4 Mn_S + 2 Si_4)	3.865 (4 Mn_I)	3.865 (4 Mn_S + 8 Si_2)	3.865 (4 Mn_I)

by the composition of the δ-layer and atomic relaxations in the neighboring silicon layers. We consider Si_{11}/Mn, in which the metallic monolayers are separated by 11 Si layers. This corresponds to a nominal bulk Mn-concentration of 10%. In the case of $N = 11$, the positions of Si atoms close to the metallic layers differ weakly from that seen in samples with $N > 11$. Thus, the magnetic properties of the Mn ML in $Si_{N\geqslant 11}/Mn$ are expected to be similar. Indeed, the calculated values of the cumulative exchange parameters $J_0 = \sum_{i\neq 0} J_{0i}$ for $N = 11,15,19$, and 23 atomic layers differ less than 4.5%, which changes the critical temperatures only by several Kelvins. In the unrelaxed Si_{11}/Mn heterostructures, the Mn atoms have four Si nearest neighbors (N2) of the adjacent Si planes at the distance 2.367 Å for all considered structural models (see Table I). The next nearest neighbors (N3) to Mn are different depending on the model used. Interestingly, in Si/Mn_S, the N3 atoms are exactly at the same distance of 3.865 Å to Mn_S as N4 atoms to Mn_I in Si_N/Mn_I and as N4 atoms to both types of Mn for the model IS. After relaxation the Si atoms change their distances to Mn, as shown in Table II, in which computed coordination spheres are collected up to the fourth neighbors for each Si_{11}/Mn model. As was mentioned above, the relaxed N2 distances increased compared to that of the unrelaxed structures for the Mn_S and Mn_I, whereas the IS model yields the opposite effect. Obviously, the structural changes define the changes in the electronic and magnetic properties of Si/Mn heterostructures.

IV. MAGNETIC PROPERTIES AND EXCHANGE INTERACTIONS

In this section we report on magnetic properties of Si/Mn heterostructures (in the following the subscript "11" is omitted). The structural information, obtained with the VASP code, was utilized for calculations of the corresponding electronic structure and exchange parameters using the KKR Green function method.

The local magnetic moments of Mn atoms in Si/Mn, calculated for the unrelaxed and relaxed geometries in FM and DLM states, are shown in Tables I and II. The magnetic moment of Mn_S is generally less affected by structural relaxations than that of Mn_I. This can be explained by the different crystallographic environment of these atoms.

A. Si/Mn_S DMA

Our results for electronic structure calculations for Si/Mn_S are in a very good agreement with the pioneering work of Qian *et al.*[40] The calculated densities of states (DOS), obtained for FM and DLM reference states, are shown in Figs. 3, 4, and 5(a). The DOS exhibits the half-metallic character with a small gap in the minority channel of about 0.1 eV. The bonding d_{xy}, d_{z^2}, and $d_{x^2-y^2}$ states of Mn_S hybridize strongly with the p states of the nearest Si layers developing a peak at the Fermi level in the majority spin channel. The nonbonding Mn_S d_{xz} and d_{yz} are concentrated in a narrow band with the bandwidth of about 1 eV at 2.5 eV below the Fermi level. The antibonding Mn_S d_{xy}, d_{z^2}, and $d_{x^2-y^2}$ and Si p states in the minority channel form the conduction bands. The exchange splitting is approximately 3 eV. In the DLM state [Fig. 5(a)], the DOS is getting broader, and as a result, the local magnetic moment of Mn decreases slightly and the system is getting metallic.

A schematic representation of the exchange interactions between the Mn atoms calculated with the KKR method is given in Fig. 6. The values of the exchange parameters, obtained for both FM and DLM reference states, are shown in Figs. 7(a) and 7(b). For the FM reference state, the exchange interaction between the first nearest neighbors $J_{01} =$ 26.3 meV is large and positive, demonstrating the robust trend to ferromagnetism in these materials. The interactions between the second and more distant neighbors are much

TABLE II. The same as Table I but for relaxed Si_{11}/Mn_S, Si_{11}/Mn_I, and Si_{11}/Mn_{IS}.

				Si_{11}/Mn_{IS}	
		Si_{11}/Mn_S	Si_{11}/Mn_I	Mn_S	Mn_I
m (μ_B)	FM	3.215	2.796	2.597	1.423
	DLM	3.172	2.531	2.522	2.277
R (Å)	N2	2.398 (4 Si_1)	2.419 (4 Si_1)	2.341 (4 Si_1)	2.341 (4 Si_1)
	N3	3.865 (4 Mn_S)	2.733 (4 Si_0)	2.733(4 Mn_I)	2.692 (2 Si_2)
	N4	3.889 (8 Si_2)	2.795 (2 Si_2)	3.836 (8 Si_2)	2.733 (4 Mn_S)
	N5	5.466 (4 Mn_S)	3.865 (4 Mn_I)	3.865 (4 Mn_S)	3.865 (4 Mn_I)

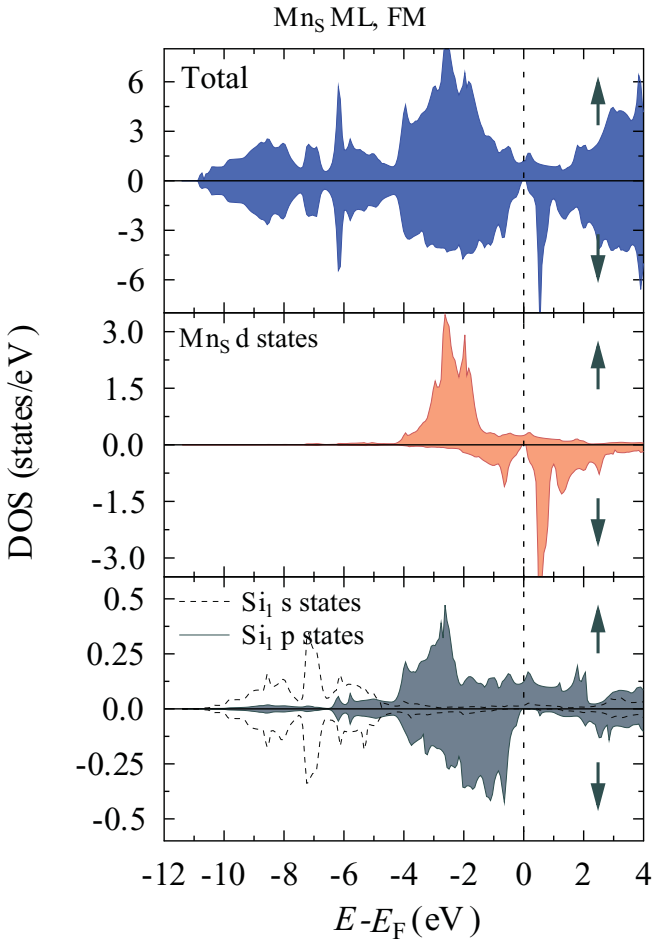

FIG. 3. (Color online) Calculated spin-polarized total and atom-resolved DOS for the Si/Mn$_S$ heterostructure in the FM state. Si$_1$ refers to an atom belonging to a silicon layer nearest to the Mn ML. The partial s and p DOS are shown for Si$_1$ with dashed and solid lines. Majority DOS are plotted as positive values, minority DOS as negative ones. The vertical dashed line indicates the Fermi energy.

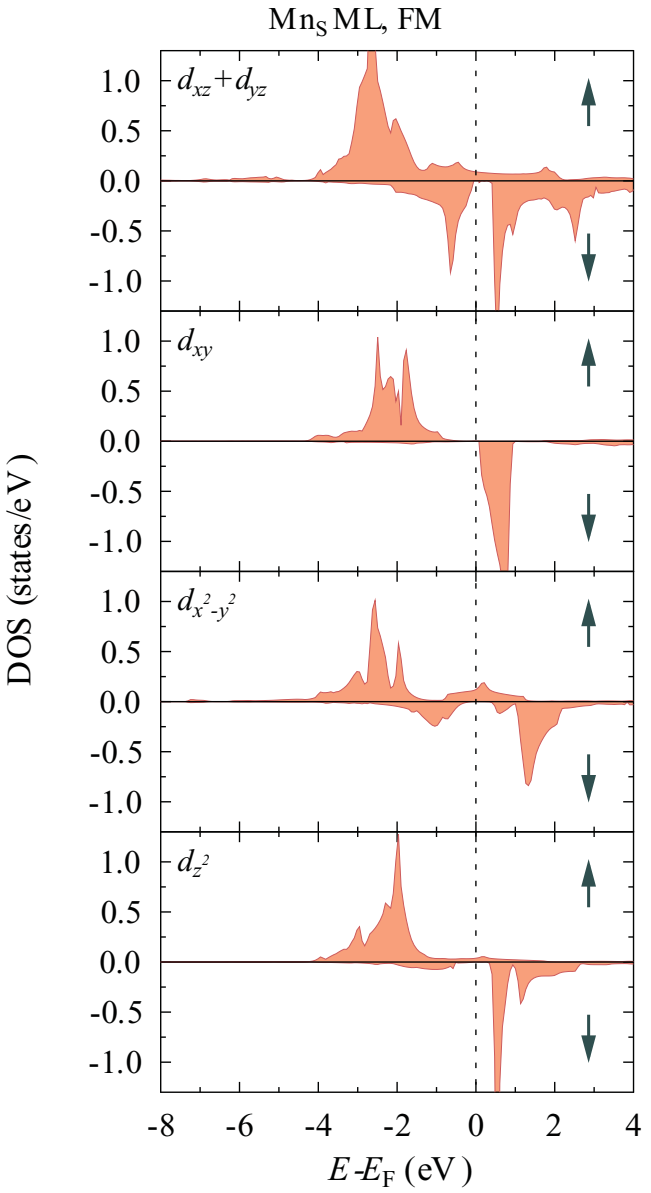

FIG. 4. (Color online) Calculated spin-resolved Mn d DOS in the Si/Mn$_S$ heterostructure in the FM state. The majority DOS are plotted as positive values, minority DOS as negative ones. The vertical dashed line indicates the Fermi energy.

weaker and quickly vanish with increasing distances. The DLM results have the same trend with slightly reduced values of the exchange parameters. Thus, our calculations support the conclusion of the work of Qian *et al.*,[40] that the Si/Mn$_S$ heterostructures are stable FM systems. A similar type of the exchange interactions was recently found in Ge/Mn$_S$ DMA.[28,42,43,45,46]

B. Si/Mn$_I$ DMA

Next we consider the case of Si/Mn$_I$ in FM and DLM states. Si atoms are lying in this structure in the same (001) plane as Mn$_I$ atoms and the character of the hybridization changes completely.[41] As is seen from the computed spin- and atom-resolved DOS [Figs. 5(b), 8, and 9], there is strong hybridization between the Mn$_I$ d_{xy}, d_{xz}, and d_{yz} and Si$_0$ p states. On the other hand, d_{z^2} and $d_{x^2-y^2}$ hybridize with the p states of Si$_1$ and Si$_2$ planes (interplane bonding) since the corresponding interatomic distances are relatively small (2.419 Å and 2.795 Å; see Fig. 1 and Table II). Due to such a strong hybridization, the system is metallic, showing a broad DOS in both spin channels. Since the d states of Mn$_I$ are more occupied than that in Si/Mn$_S$, the local magnetic moment is smaller than that in the substitutional position. In the DLM state, the Mn$_I$ d_{z^2} and $d_{x^2-y^2}$ are narrower than in the FM state, while the bandwidth of the d_{xy}, d_{xz}, and d_{yz} states is larger than that of the FM reference state. Because of the narrow d_{z^2} and $d_{x^2-y^2}$ bands, the DLM local magnetic moment of Mn$_I$ is smaller by about $0.27\mu_B$ than in FM state.

The exchange interactions in Si/Mn$_I$ are much more complex than in the case of Si/Mn$_S$. In the FM reference state [Fig. 7(c)], the exchange interactions between the first and the second nearest neighbors are of almost the same magnitude but of the opposite signs: $J_{01} = 19.97$ meV and $J_{02} = -24.41$ meV, respectively. The interactions with more

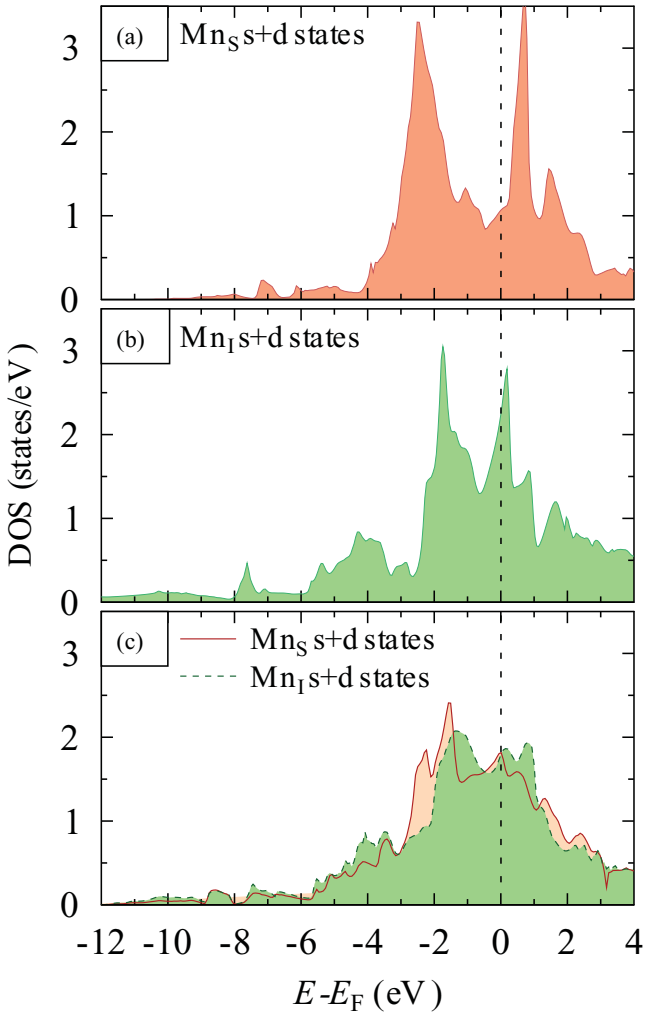

FIG. 5. (Color online) Calculated DLM DOS in majority spin channel of Mn s and d states in Si/Mn$_S$ (a), Si/Mn$_I$ (b), and Si/Mn$_{IS}$ (c) heterostructures. The vertical dashed line indicates the Fermi energy.

distant atoms are much smaller. The strong antiferromagnetic (AFM) coupling with the second neighbors is due to the superexchange interaction between Mn$_I$ magnetic cations through the Si$_0$ anion, which lies in the middle of the Mn$_I$-Mn$_I$ connection. Otherwise, the Si$_0$ anion establishes a 90° FM superexchange interaction between the nearest Mn$_I$ cations. In this situation, the different types of exchange interaction compete with each other and the ferromagnetism is not stable anymore. The DLM simulations yield the same trend, although the magnitudes of J_{ij} are substantially smaller than that in the FM reference state [see Fig. 7(d)]. Additionally, the magnitude of J_{01} (3.48 meV) is only about half of J_{02} (−6.84 meV). This indicates that the ground state might be noncollinear. This result for Si/Mn$_I$ DMA differs from the result of the recent study of the Ge/Mn$_I$ DMA, which was found to be ferromagnetic.[45]

C. Si/Mn$_{IS}$ DMA

In Si/Mn$_{IS}$ DMA, the d electrons of the substitutional and interstitial Mn atoms form strong metallic bonds in the (001) plane [see Figs. 5(c), 10, and 11]. They participate as

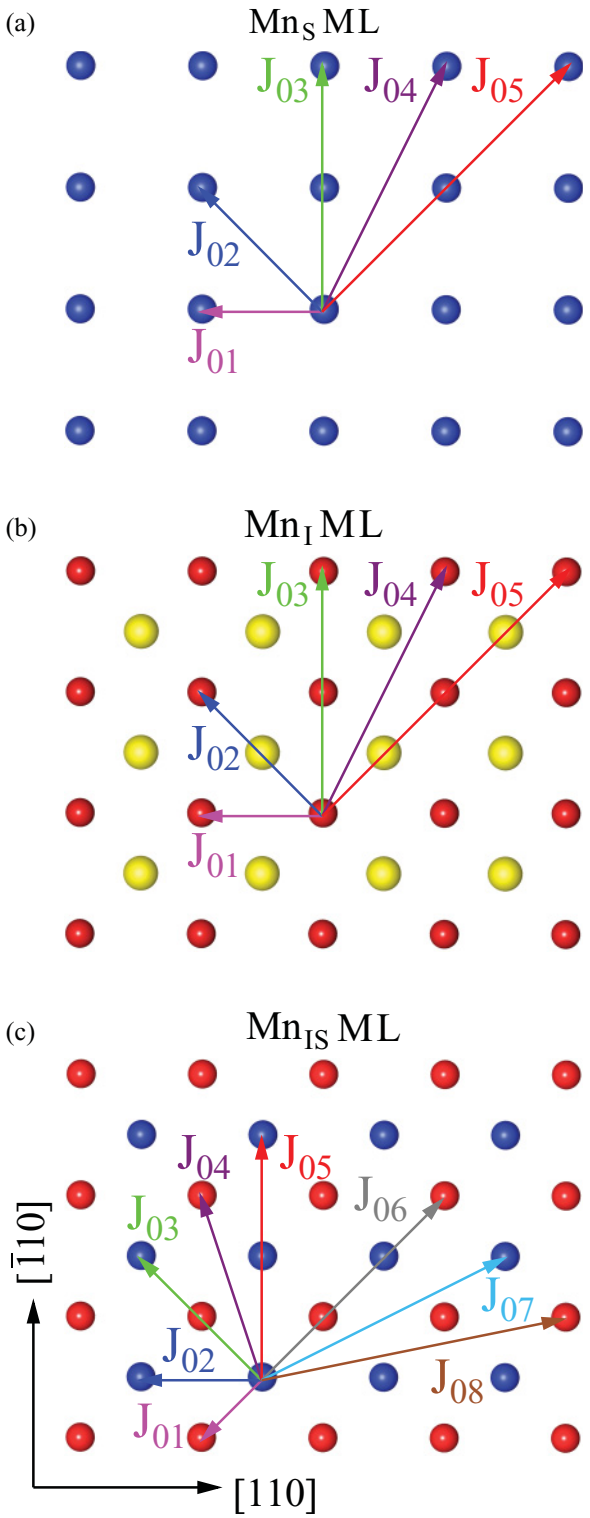

FIG. 6. (Color online) Schematic representation of magnetic interactions in (001) plane of Si/Mn heterostructures. J_{01} denotes the exchange interaction of the Mn atom with the nearest neighbors, J_{02} refers to the exchange interaction with the next nearest neighbors, and so on.

well in the hybridization with p electrons of the adjacent Si layers; this hybridization is stronger than that in Si/Mn$_S$ and Si/Mn$_I$ DMA. As a result, the Si adjacent layers are metallic in both spin channels. Due to the strong d-d hybridization

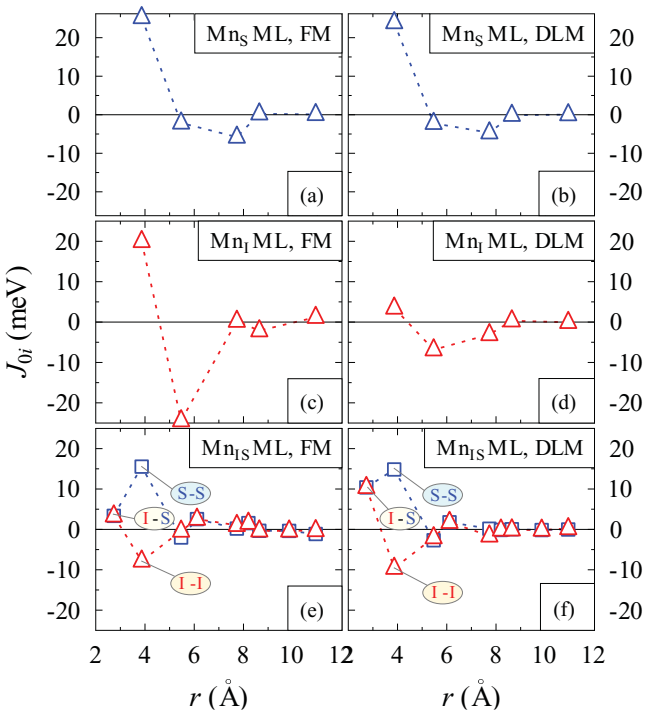

FIG. 7. (Color online) Exchange parameters for Si/Mn calculated in FM and DLM reference states.

in the manganese plane the magnetic moments are smaller in comparison with Si/Mn$_S$ and Si/Mn$_I$ systems. In the DLM reference state, the bandwidth of the Mn$_S$ d states increases, and therefore the corresponding local magnetic moment is smaller than that in the FM state. For the interstitial Mn one has the opposite effect in the DLM state: the d states are getting broader thereby increasing the value of the local magnetic moment (see Table II).

The exchange interactions in the Si/Mn$_{IS}$ are characterized by the strong d-d hybridization of Mn atoms and by the superexchange mechanism through the adjacent Si layers. The exchange interaction between the nearest substitutional Mn atoms is positive in both FM and DLM states [$J^{FM}_{S\text{-}S} = 15.54$ meV and $J^{DLM}_{S\text{-}S} = 14.84$ meV, respectively; see Figs. 7(e) and 7(f)], while that between the nearest interstitial atoms is negative ($J^{FM}_{I\text{-}I} = -7.8$ meV and $J^{DLM}_{I\text{-}I} = -9.6$ meV). It is interesting that these intrasublattice exchange parameters depend weakly on the reference state. The interaction between the nearest substitutional and interstitial magnetic moments (intersublattice interaction) is positive and its magnitude is substantially different in the FM and DLM reference states ($J^{FM}_{I\text{-}S} = 3.32$ meV and $J^{DLM}_{I\text{-}S} = 10.4$ meV, respectively).

Since $|J^{FM}_{I\text{-}I}| > |J^{FM}_{I\text{-}S}|$ and $J^{FM}_{I\text{-}I}$ is negative, we conclude that the FM state is not energetically favorable in this system at low temperatures. The competition between intersublattice and Mn$_I$ intrasublattice magnetic interactions leads to a noncollinear magnetic order in the system. The relatively large and positive intersublattice exchange parameter in the DLM state indicates possible FM fluctuations for the high-temperature case.

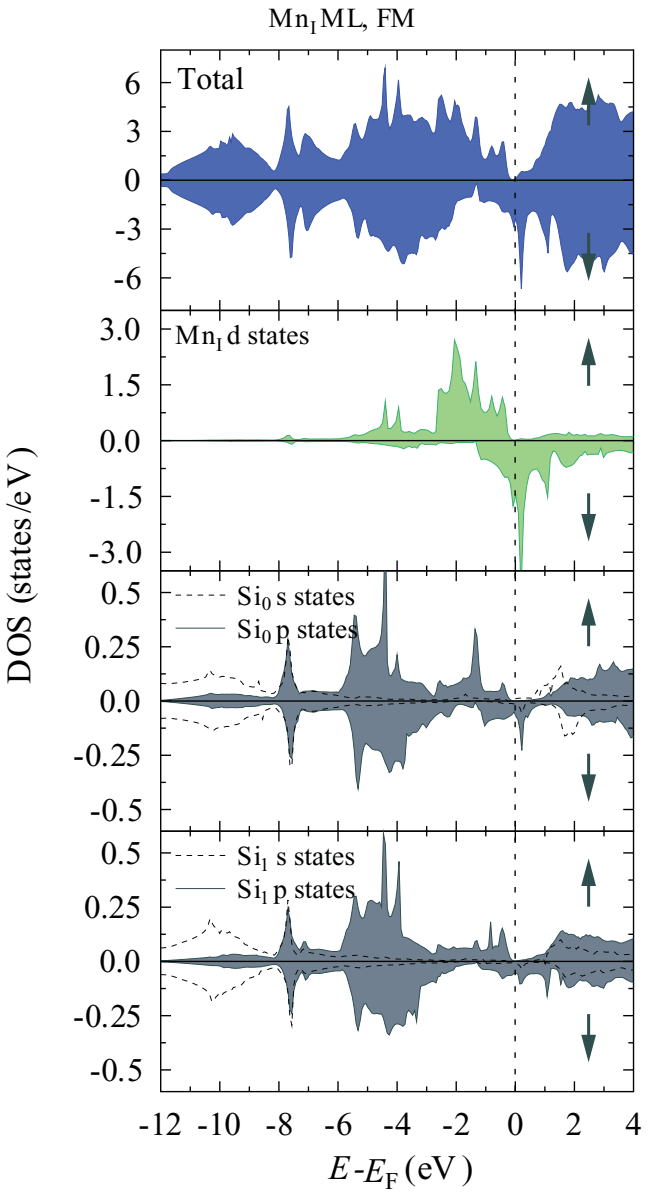

FIG. 8. (Color online) Calculated spin-polarized total and atom-resolved DOS for the Si/Mn$_I$ heterostructure in the FM state. Si$_0$ denotes the Si atom being in the same layer as Mn$_I$. Si$_1$ refers to the atom belonging to the silicon layer nearest to the Mn ML. The partial s and p DOS are shown for Si with dashed and solid lines. Majority DOS are plotted as positive values, minority DOS as negative ones. The vertical dashed line indicates the Fermi energy.

V. MAGNON SPECTRA AND CRITICAL TEMPERATURE OF FM ORDERING IN SI/MN DMAS

The magnon spectra for the Mn$_S$, Mn$_I$, and Mn$_{IS}$ ML in the Si/Mn DMA, calculated using the exchange parameters obtained in the FM and DLM reference states, are shown in Fig. 12. The magnon frequencies of the Si/Mn$_S$ are positive for both FM and DLM reference states [see Figs. 12(a) and 12(b)], which allows us to identify the stable FM order as the spin ground state.

In the case of the Si/Mn$_I$ DMA, there appear magnons with negative energies [Figs. 12(c) and 12(d)], indicating that the

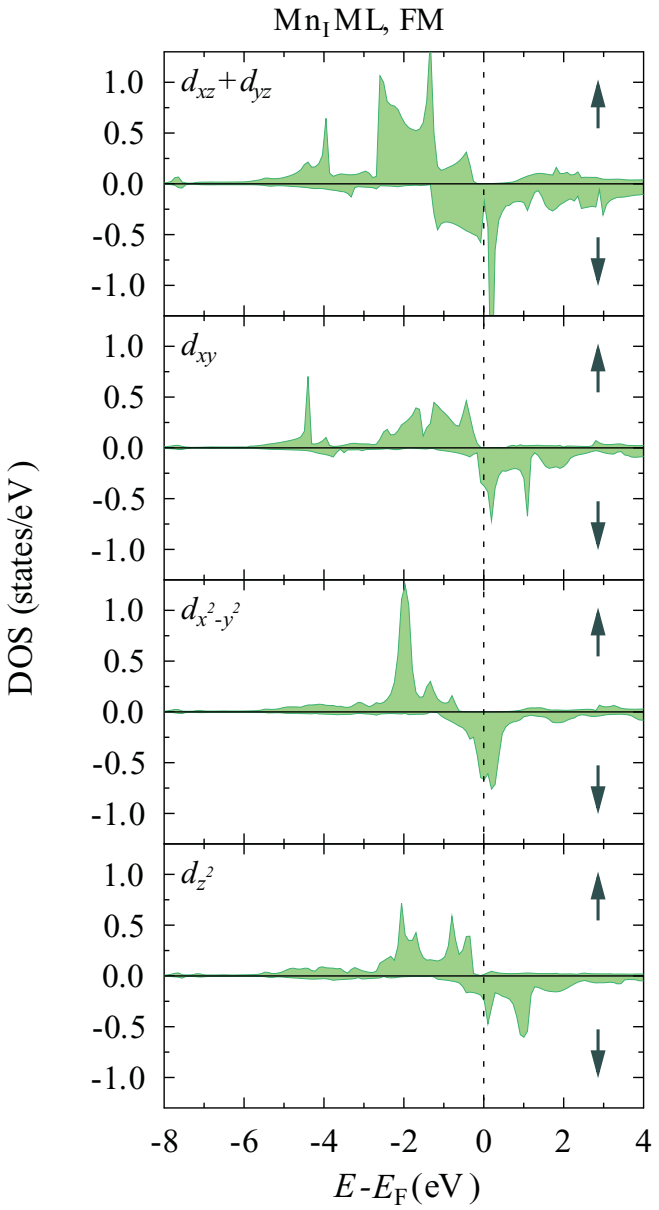

FIG. 9. (Color online) Calculated spin-resolved partial DOS of Mn d electrons in the Si/Mn$_I$ heterostructure in the FM state. Majority DOS are plotted as positive values, minority DOS as negative ones. The vertical dashed line indicates the Fermi energy.

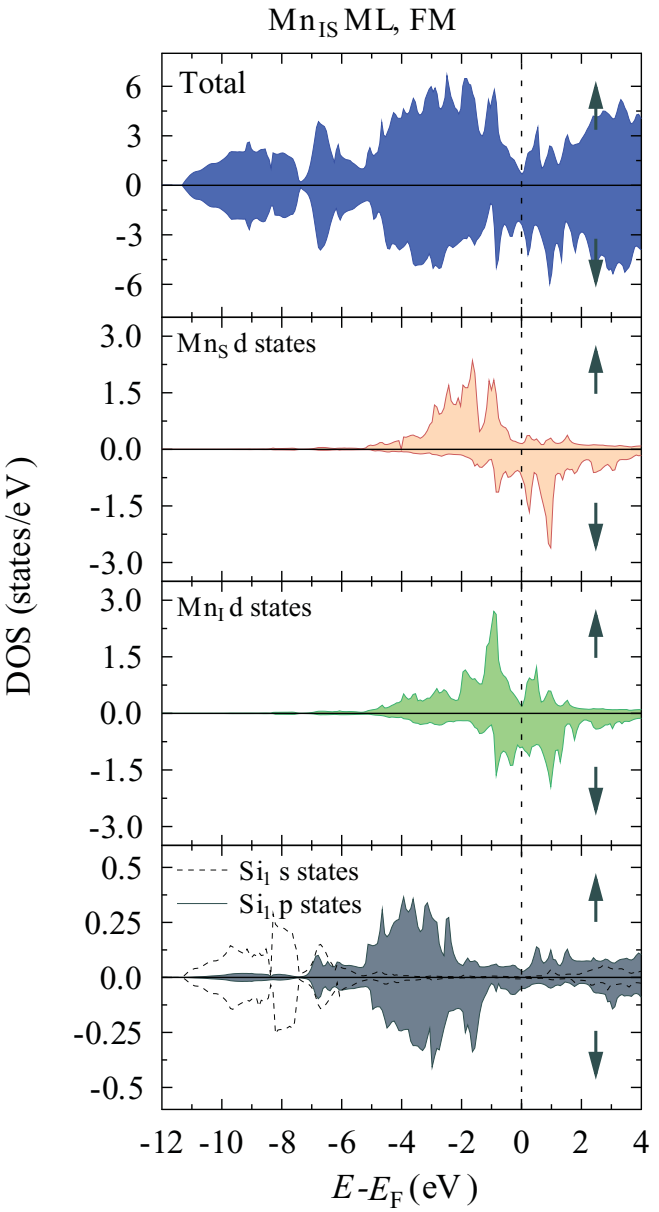

FIG. 10. (Color online) Calculated spin-polarized total and atom-resolved DOS for the Si/Mn$_{IS}$ heterostructure in the FM state. Si$_1$ refers to the atom belonging to the silicon layer nearest to the Mn ML. The partial s and p DOS are shown for Si with dashed and solid lines. Majority DOS are plotted as positive values, minority DOS as negative ones. The vertical dashed line indicates the Fermi energy.

FM state is not energetically favorable. The shapes of magnon dispersions in the FM and DLM states are similar, although the DLM energies are significantly smaller. The minimum of the magnon dispersion around the $\bar{X}$ could indicate the presence of a collinear AFM stripe phase. However, explicit calculations using the latter as the starting point (not shown) prove that it is not a true ground state, either. This hints at a noncollinear ground state. The reason for this is a strong competition between J_{01} and J_{02}, which are of the same order but are different in sign. In the DLM state, this competition seems to be stronger, which results in the two minima of comparable depth in the dispersion. They are located around $\mathbf{q} \approx 0.41\bar{\Gamma}\bar{M}$ and $\mathbf{q} \approx 0.85\bar{M}\bar{X}$.

Since in the Si/Mn$_{IS}$ DMA there are two magnetic sublattices, the corresponding magnon spectra consist of acoustic and optical branches [see Figs. 12(e) and 12(f)]. In both FM and DLM reference states, the acoustic branch features negative magnon frequencies with the minimum at $\bar{M} = (\pi/a_{Si}, \pi/a_{Si})$ point. The instability arises due to the strong negative exchange interaction between nearest Mn$_I$ moments. The spin waves in both reference states indicate a noncollinear magnetic order, again due to strong competing exchange interactions.

The exchange parameters J_{ij} defined by Eq. (2) can be used to estimate the critical temperature of magnetic ordering in Si/Mn DMAs. We resort to the Monte Carlo (MC) simulations

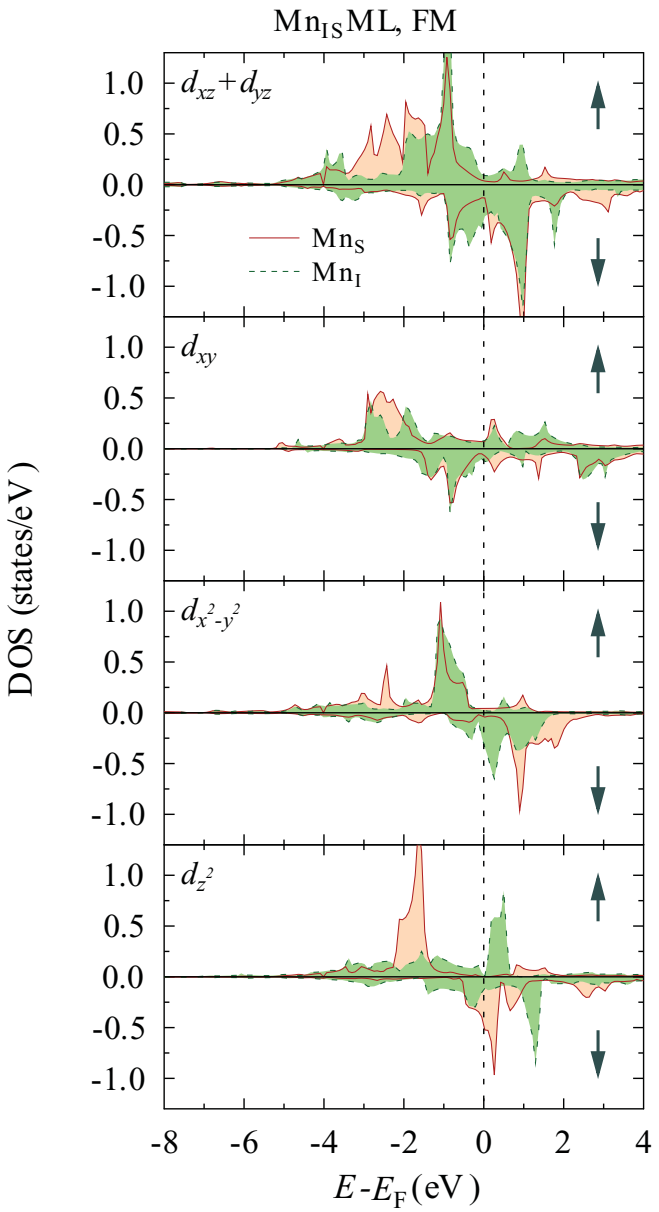

FIG. 11. (Color online) Calculated spin-resolved partial DOS of Mn d electrons in the Si/Mn$_{IS}$ heterostructure in the FM state. Majority DOS are plotted as positive values, minority DOS as negative ones. The vertical dashed line indicates the Fermi energy.

within the effective Heisenberg Hamiltonian,

$$H = -\sum_{i,j} J_{ij}\mathbf{e}_i \cdot \mathbf{e}_j, \tag{2}$$

where $\mathbf{e}_i$ is a unit vector parallel to the magnetic moment at site i. The quasi two-dimensional character of our systems pose several difficulties in a straightforward use of the above Hamiltonian. If we neglect interlayer exchange, i.e., take all Mn MLs as magnetically independent, Mermin-Wagner theorem[61,62] excludes the possibility of FM order at finite temperature in the two-dimensional Heisenberg model without magnetic anisotropy. Ferromagnetic order in Hamiltonian Eq. (2) is unstable and destroyed by the long-range spin fluctuations. In the frame of a nonrelativistic approach, we

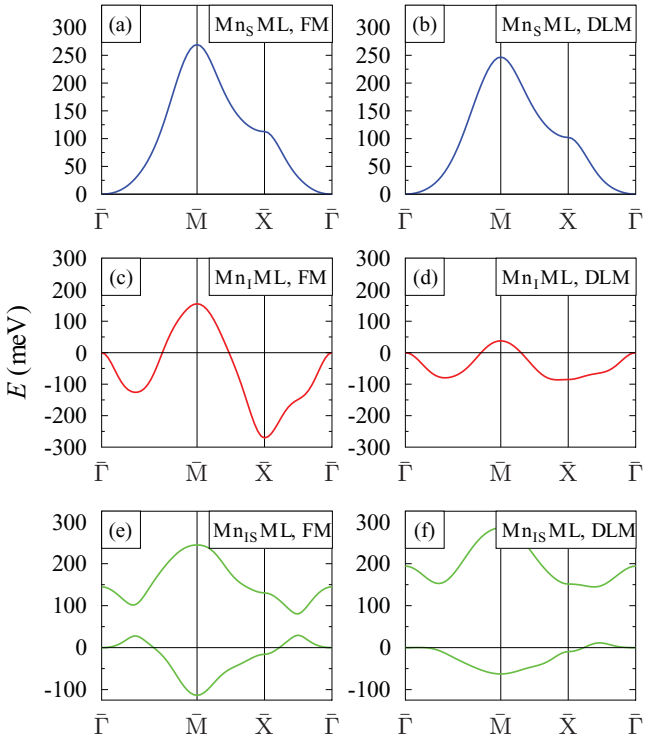

FIG. 12. (Color online) Calculated magnon spectra along $\bar{\Gamma}$–$\bar{M}$–$\bar{X}$–$\bar{\Gamma}$ directions in the first two-dimensional BZ for Si/Mn$_S$ DMA (a, b), Si/Mn$_I$ DMA (c, d), and Si/Mn$_{IS}$ DMA (e, f). The high symmetry points have the following coordinates: $\bar{\Gamma}$ (0, 0), $\bar{M}$ (π/a_{Si}, π/a_{Si}), $\bar{X}$ (π/a_{Si}, 0). The figures on the left-hand side show the magnon spectra calculated in the FM reference state, while on the right side the corresponding DLM calculations are presented.

are unable to treat correctly effects of magnetic anisotropy in Si/Mn DMAs. At a phenomenological level, we can account for the anisotropy of the system by adding a term $-\sum_i \Delta(e_i^z)^2$ in the Hamiltonian Eq. (2), where Δ is the energy of magnetic anisotropy. This term describes a magnetic system with an easy-axis ($\Delta > 0$) or easy-plane ($\Delta < 0$) anisotropy. Since the value and even the sign of the magnetic anisotropy energy is not known for Si/Mn DMAs, the energy Δ was used as parameter in our simulations.

Let us first consider the easy-axis situation, when the role of long-range spin fluctuations is effectively suppressed. In this case, it is possible to qualitatively associate a critical temperature of FM ordering obtained from MC simulation with the Curie temperature. Our MC simulations were carried out for Mn supercells with up to 7200 atoms starting from high-temperature disordered state, as described in the Ref. 63. For each temperature the thermal equilibrium was assumed to be reached after 15×10^3 MC steps, while for the determination of thermal averages over 25×10^3 MC steps were required. The MC simulations were performed for several values of Δ. The critical temperatures were estimated from the temperature dependence of the specific heat for different lattice sizes.

Our calculations show that above a certain critical value the magnitude of Δ influences the critical temperature of magnetic ordering only weakly, therefore we took the energy of magnetic anisotropy to be 0.5 and 1.0 meV monitoring the estimated critical temperature with the value of Δ; the critical

TABLE III. Critical temperatures T_C (K) estimated in the FM and DLM reference states using the magnetic anisotropy energies $\Delta =$ 0.5 and 1.0 meV in the Heisenberg model [Eq. (2)].

	Δ	Si/Mn_S	Si/Mn_I	Si/Mn_{IS}
FM	0.5	161	684	116
	1.0	175	695	122
DLM	0.5	134	50	244
	1.0	141	54	250

temperatures are presented in Table III. The T_C estimated for $\Delta = 1.0$ meV differ only in a few Kelvin from the case of $\Delta = 0.5$ meV. On the other hand, the critical temperatures estimated from the exchange parameters calculated from the FM and DLM reference states differ rather strongly. In Si/Mn_S and Si/Mn_I DMA, the DLM T_C are smaller than that obtained with J_{ij} from the FM state, while in Si/Mn_{IS} the DLM critical temperature is almost two times larger than the T_C in the FM reference state. This can be explained by the difference of the corresponding exchange parameters. This fact is also reflected in the magnon spectra (see Fig. 12).

Now, let us qualitatively analyze the easy-plane situation. If the in-plane anisotropy is very strong, the system can be described in terms of a two-dimensional XY model. Within this framework the second-order phase transition is not possible, since the long-range spin fluctuations destroy FM phase. However, at low temperatures, there is a quasi-ordered phase with a correlation function of spins which decreases with the distance like a temperature-dependent power. The transition from the high-temperature disordered phase with the exponentially decaying correlation of spins to the low-temperature quasi-ordered phase is the Berezinskii-Kosterlitz-Thouless (BKT) transition.[64–66] The characteristic temperature associated with this transition (so-called *crossover* temperature) can be roughly estimated using the calculated exchange parameters. According to our MC simulations for the case of easy-plane anisotropy, crossover temperatures are very close to the critical temperatures obtained for the case of the easy-axis anisotropy, shown in Table III. However, the study of the BKT phase transition by means of the MC method is a difficult task because of the finite size of the simulation domain. Alternatively, the crossover temperature can be approximately calculated from the relation $T_{BKT} \approx 0.894\, J_{01}/k_B$, derived by fitting of susceptibility and correlation length data, obtained with MC method, to the BKT form.[67] Here, J_{01} is the exchange parameter describing the interaction with nearest-neighbor spins and k_B is the Boltzmann constant. In the case of Si/Mn_S DMA the exchange parameter $J_{01} \approx 25$ meV yields the crossover temperature of 259 K, which is higher than that obtained with MC method. A more detailed investigation of this problem is beyond the scope of the given paper.

VI. CONCLUSION

The electronic and magnetic properties of Si/Mn digital alloys, obtained by the insertion of Mn monolayers in the Si host, were studied using the first-principles KKR method within the density functional theory. Three various structures of the Mn monolayer were considered: manganese atoms occupy substitutional (i), interstitial (ii), and both substitutional and interstitial (iii) positions. The electronic and magnetic properties were found to be strongly dependent on the underlying crystal structure. According to our study, the Si/Mn_S DMA is a stable FM system. In the case of the Si/Mn_I DMA, the magnetic order is noncollinear with a tendency to an AFM structure along [010] direction. The main reason for the noncollinear magnetic order is a competition between a FM exchange interaction of the two nearest Mn magnetic moments and a strong AFM superexchange of the two next-nearest neighboring Mn atoms via Si. In the Si/Mn_{IS} DMA, a complex magnetic order is found and may strongly depend on temperature. The character of the exchange interactions in this system indicates possible complex magnetic structures due to a strong AFM coupling in the interstitial sublattice.

ACKNOWLEDGMENTS

This work is supported by the Sonderforschungsbereich SFB 762, "Functionality of Oxidic Interfaces." We acknowledge the support of the Federal Targeted Program "Scientific and scientific—pedagogical personnel of innovative Russia in 2009-2013"and of the University of the Basque Country [Proyecto GV-UPV/EHU (Grant No. IT-366-07), Spanish Ministerio de Ciencia y Tecnología (Grant No. FIS2010-19609-C02-01)]. This work was supported in part by the Russian Foundation for Basic Research, Project Nos. 10-02-00118 and 10-02-01110. The calculations were performed at the Rechenzentrum Garching of the Max Planck Society (Germany) and at SKIF Cyberia cluster in Tomsk (Russia).

*aernst@mpi-halle.de

[1] E. R. Weber, Appl. Phys. A **30**, 1 (1983).
[2] D. Gilles, W. Schröter, and W. Bergholz, Phys. Rev. B **41**, 5770 (1990).
[3] D. Shinoda and S. Asanabe, J. Phys. Soc. Jpn. **21**, 555 (1966).
[4] H. J. Williams, J. H. Wernick, R. C. Sherwood, and G. K. Wertheim, J. Appl. Phys. **37**, 1256 (1966).
[5] P. Lengsfeld, S. Brehme, G. Ehlers, H. Lange, N. Stüsser, Y. Tomm, and W. Fuhs, Phys. Rev. B **58**, 16154 (1998).
[6] Y. Ishikawa, T. Komatsubara, and D. Bloch, Physica B + C **86-88**, 401 (1977).
[7] T. Jungwirth, J. Sinova, J. Mašek, J. Kučera, and A. H. MacDonald, Rev. Mod. Phys. **78**, 809 (2006).
[8] T. Dietl, in *Modern Aspects of Spin Physics*, Lecture Notes in Physics, Vol. 712, edited by W. Pötz, U. Hohenester, and J. Fabian (Springer, Berlin/Heidelberg, 2007), pp. 1–46.
[9] K. Sato *et al.*, Rev. Mod. Phys. **82**, 1633 (2010).
[10] M. Bolduc, C. Awo-Affouda, A. Stollenwerk, M. B. Huang, F. G. Ramos, G. Agnello, and V. P. LaBella, Phys. Rev. B **71**, 033302 (2005).
[11] A. Wolska, K. Lawniczak-Jablonska, M. Klepka, M. S. Walczak, and A. Misiuk, Phys. Rev. B **75**, 113201 (2007).

[12]S. Zhou *et al*., Phys. Rev. B **75**, 085203 (2007).
[13]L. Zeng, E. Helgren, M. Rahimi, F. Hellman, R. Islam, B. J. Wilkens, R. J. Culbertson, and D. J. Smith, Phys. Rev. B **77**, 073306 (2008).
[14]V. N. Men'shov, V. V. Tugushev, S. Caprara, and E. V. Chulkov, Phys. Rev. B **83**, 035201 (2011).
[15]T. Dubroca, J. Hack, R. E. Hummel, and A. Angerhofer, Appl. Phys. Lett. **88**, 182504 (2006).
[16]A. Orlov *et al*., JETP **109**, 602 (2009).
[17]J. J. Harris, J. Mater. Sci.: Mater. Electron. **4**, 93 (1993).
[18]A. M. Nazmul, T. Amemiya, Y. Shuto, S. Sugahara, and M. Tanaka, Phys. Rev. Lett. **95**, 017201 (2005).
[19]S. Azatyan, M. Iwami, and V. Lifshits, Surf. Sci. **589**, 106 (2005).
[20]M. R. Krause, A. J. Stollenwerk, J. Reed, V. P. LaBella, M. Hortamani, P. Kratzer, and M. Scheffler, Phys. Rev. B **75**, 205326 (2007).
[21]M. B. Reakes, C. Eames, and S. P. Tear, J. Phys. Condens. Matter **21**, 265001 (2009).
[22]C. Nolph, E. Vescovo, and P. Reinke, Appl. Surf. Sci. **255**, 7642 (2009).
[23]H. Wu, M. Hortamani, P. Kratzer, and M. Scheffler, Phys. Rev. Lett. **92**, 237202 (2004).
[24]H. Wu, P. Kratzer, and M. Scheffler, Phys. Rev. B **72**, 144425 (2005).
[25]M. Hortamani, H. Wu, P. Kratzer, and M. Scheffler, Phys. Rev. B **74**, 205305 (2006).
[26]J. A. Gardener *et al*., Nanotechnology **21**, 025304 (2010).
[27]S. H. Chiu, H. S. Hsu, and J. C. A. Huang, J. Appl. Phys. **103**, 07D110 (2008).
[28]A. Continenza, F. Antoniella, and S. Picozzi, Phys. Rev. B **70**, 035310 (2004).
[29]V. N. Men'shov, V. V. Tugushev, P. M. Echenique, S. Caprara, and E. V. Chulkov, Phys. Rev. B **78**, 024438 (2008).
[30]S. Caprara, V. V. Tugushev, P. M. Echenique, and E. V. Chulkov, Europhys. Lett. **85**, 27006 (2009).
[31]S. Caprara, V. V. Tugushev, and E. V. Chulkov, Phys. Rev. B **84**, 085311 (2011).
[32]V. F. Sapega, A. Trampert, and K. H. Ploog, Phys. Rev. B **77**, 245301 (2008).
[33]B. Aronzon, A. Lagutin, V. Rylkov, V. Tugushev, V. Menshov, A. Lashkul, R. Laiho, O. Vikhrova, Y. Danilov, and B. Zvonkov, JETP Lett. **87**, 164 (2008).
[34]V. N. Men'shov, V. V. Tugushev, S. Caprara, P. M. Echenique, and E. V. Chulkov, Phys. Rev. B **80**, 035315 (2009).
[35]X. Chen *et al*., Appl. Phys. Lett. **81**, 511 (2002).
[36]A. Stroppa, X. Duan, M. Peressi, D. Furlanetto, and S. Modesti, Phys. Rev. B **75**, 195335 (2007).
[37]J. K. Garleff, C. Çelebi, W. Van Roy, J.-M. Tang, M. E. Flatté, and P. M. Koenraad, Phys. Rev. B **78**, 075313 (2008).
[38]A. Stroppa, G. Kresse, and A. Continenza, Phys. Rev. B **83**, 085201 (2011).
[39]D. A. Rowlands, A. Ernst, B. L. Györffy, and J. B. Staunton, Phys. Rev. B **73**, 165122 (2006).
[40]M. C. Qian, C. Y. Fong, K. Liu, W. E. Pickett, J. E. Pask, and L. H. Yang, Phys. Rev. Lett. **96**, 027211 (2006).
[41]H. Wu, P. Kratzer, and M. Scheffler, Phys. Rev. Lett. **98**, 117202 (2007).
[42]S. Picozzi, M. Ležaić, and S. Blügel, Phys. Status Solidi A **203**, 2738 (2006).
[43]H.-Y. Wang and M. C. Qian, J. Appl. Phys. **99**, 08D705 (2006).
[44]Y. A. Uspenskii and E. T. Kulatov, J. Magn. Magn. Mater. **321**, 931 (2009).
[45]M. M. Otrokov, A. Ernst, S. Ostanin, G. Fischer, P. Buczek, L. M. Sandratskii, W. Hergert, I. Mertig, V. M. Kuznetsov, and E. V. Chulkov, Phys. Rev. B **83**, 155203 (2011).
[46]M. M. Otrokov, V. V. Tugushev, A. Ernst, S. A. Ostanin, V. M. Kuznetsov, and E. V. Chulkov, JETP **112**, 625 (2011).
[47]P. Buczek, A. Ernst, P. Bruno, and L. M. Sandratskii, Phys. Rev. Lett. **102**, 247206 (2009).
[48]M. Hortamani, L. Sandratskii, P. Kratzer, I. Mertig, and M. Scheffler, Phys. Rev. B **78**, 104402 (2008).
[49]G. Kresse and J. Hafner, Phys. Rev. B **49**, 14251 (1994).
[50]G. Kresse and J. Furthmüller, Phys. Rev. B **54**, 11169 (1996).
[51]J. Hafner, J. Comput. Chem. **29**, 2044 (2008).
[52]J. P. Perdew, K. Burke, and M. Ernzerhof, Phys. Rev. Lett. **77**, 3865 (1996).
[53]P. E. Blöchl, Phys. Rev. B **50**, 17953 (1994).
[54]H. J. Monkhorst and J. D. Pack, Phys. Rev. B **13**, 5188 (1976).
[55]M. Luders, A. Ernst, W. M. Temmerman, Z. Szotek, and P. J. Durham, J. Phys. Condens. Matter **13**, 8587 (2001).
[56]B. L. Gyorffy, Phys. Rev. B **5**, 2382 (1972).
[57]T. Oguchi, K. Terakura, and N. Hamada, J. Phys. F **13**, 145 (1983).
[58]A. I. Liechtenstein, M. I. Katsnelson, V. P. Antropov, and V. A. Gubanov, J. Magn. Magn. Mater. **67**, 65 (1987).
[59]S. Shallcross, A. E. Kissavos, V. Meded, and A. V. Ruban, Phys. Rev. B **72**, 104437 (2005).
[60]M. M. Otrokov, S. A. Ostanin, A. Ernst, V. M. Kuznetsov, and E. V. Chulkov, Phys. Solid State **52**, 1680 (2010).
[61]N. D. Mermin and H. Wagner, Phys. Rev. Lett. **17**, 1133 (1966).
[62]M. Bander and D. L. Mills, Phys. Rev. B **38**, 12015 (1988).
[63]G. Fischer, M. Dane, A. Ernst, P. Bruno, M. Lueders, Z. Szotek, W. Temmerman, and W. Hergert, Phys. Rev. B **80**, 014408 (2009).
[64]V. L. Berezinskii, Sov. Phys. JETP **32**, 493 (1971).
[65]J. M. Kosterlitz and D. J. Thouless, J. Phys. C **6**, 1181 (1973).
[66]J. M. Kosterlitz, J. Phys. C **7**, 1046 (1974).
[67]R. Gupta and C. F. Baillie, Phys. Rev. B **45**, 2883 (1992).